Technical Report

Program and KPI: Sub-program 2.2 KPI 3.26

Report Title: Ultrasonic assessment of intramuscular fat percentage in beef and lamb loins at 37ºC

Prepared by: S. Hitchman[1], C. Steel[2], P. McGilchrist[2]
[1]AgResearch Pty Ltd, New Zealand
[2]The University of New England, Armidale NSW

Date published: 30 November 2022

Citation

Acknowledgements

.

Abstract

Ultrasound is an extensively studied technology for objective measurements in a range of different applications. The driving motivation behind recent improvements in ultrasonic image reconstruction for soft tissues has come from the medical industry. However, few of these improvements have translated into meat quality assessment. This work investigates quantitative ultrasound techniques to estimate the intramuscular fat content of NZ and Australian Lamb loins. This report reviews recent literature and discusses the application of novel methods for quantifying intramuscular fat content.

Contents

1 Background

There is a need for pre-slaughter estimates of intramuscular fat content in red meat. B-mode ultrasound is currently implemented on live animals to estimate marble score of red meat pre-slaughter. However, this requires trained professionals to review images in real time to estimate intramuscular fat content. This work investigates the applicability of speed of sound (SoS) measuring/mapping techniques to quantify intramuscular fat content in New Zealand beef and lamb loins. Previous work showed that at body temperature, fat has an SoS of ~1440m/s and lean muscle had a SoS of ~1580m/s. Due to the relationship between SoS and intramuscular fat content, SoS mapping could provide a tool to automatically quantify and estimate IMF%.

There is a need for pre-slaughter estimates of intramuscular fat content in red meat. B-mode ultrasound is currently implemented on live animals to estimate marble score of red meat pre-slaughter. However, this requires trained professionals to review images in real time to estimate intramuscular fat content. This work investigates the applicability of speed of sound (SoS) measuring/mapping techniques to quantify intramuscular fat content in New Zealand beef and lamb loins. Previous work showed that at body temperature, fat has an SoS of ~1440m/s and lean muscle had a SoS of ~1580m/s. Due to the relationship between SoS and intramuscular fat content, SoS mapping could provide a tool to automatically quantify and estimate IMF%.

1.1 Transmission mode ultrasound

Transmission mode ultrasound uses separate transducers as source and receivers to detect ultrasound waves that have passed through the material. Typically, the time of flight (ToF), amplitude and travel distance of the ultrasound emission between source and receiver are used to accurately measure the speed of sound and attenuation in a material.

Previous work using an ultrasound transducer/receiver A-mode system in transmission mode showed that speed of sound measurements could be used to estimate intramuscular fat percentage (IMF%) in beef (Park, Whittaker, Miller, & Hale, 1994; Whittaker, Park, Thane, Miller, & Savell, 1992). However, these techniques have not been applicable to live animal imaging due to the requirement that subcutaneous fat be removed and muscle to be cut into appropriate shapes and sizes for speed of sound calculations to be made. Appendix 0 gives an example of A-mode ultrasound in transmission mode.

More recent work has shown good correlations of speed of sound with IMF% using a penetrating probe A-mode ultrasound system, intended for use on hot carcass IMF% assessment (Bradbury, 2007). Limitations of this technique are that only the direct path of the ultrasound wave between source and receiver is measured, and it was concluded a minimum of 9 repeated measures were required to estimate total IMF%.

Ultrasound computed tomography (UCT) is an extension of transmission A-mode ultrasound which generates full field speed of sound estimates using a circular distribution of sources and receivers encompassing the material. UCT operates in transmission mode and the reconstruction of the SoS map is similar to X-ray computed tomography (CT) produces images based on density (Kim & Khambampati, 2015). This technique has successfully been applied to breast cancer imaging, however the requirement of sensors to encompass the sample limits the application of this technique to live animal imaging.

1.2 Echo (Reflection) mode

Echo or reflection mode ultrasound uses the same transducer elements as both source and receiver. In this case, scatterers in the tissue/sample reflect ultrasound waves back to the transducer elements. H. J. Young, N. T. Jenkins, Q. Zhao, and K. K. McCully (2015) used A-mode ultrasound in echo intensity to determine IMF% in several muscles of live patients. After correcting for the subcutaneous fat depth, correlations between echo intensity and IMF% ranged from .91 to .76 depending on the muscle type.

B-Mode ultrasound uses a distribution of ultrasound emitters and receivers placed on the surface of the material and is the most common form of ultrasound imaging used in medicine and agriculture. B-mode ultrasound operates in reflection/echo mode; ultrasound emissions are reflected by scatterers are used to reconstruct a subsurface map of the material via several different imaging protocols. The most common ultrasound imaging protocol used for veterinarian and medical applications is termed 'focused' imaging. Focussed imaging uses a delay in the excitation of several transducer elements to focus the resultant ultrasound wave to a specific depth in the tissue. Focussed imaging is used due to its good depth of imaging. However, to reconstruct the image from the raw data the speed of sound of the material must be assumed. Recently Plane wave imaging has been developed, which is a much faster protocol and has resulted in methods to estimate the SoS of samples in B-mode ultrasound.

Typically, a SoS of 1540m/s is used for soft tissue imaging, however this value can be changed in real time to improve the image focus. This allows for the average speed of sound in a sample to be estimated by calculating image sharpness as a function of the SoS used for image reconstruction. The SoS that produces the greatest image sharpness is an estimate of the average speed of sound of the sample. Image sharpness is usually assessed by visual inspection by the ultrasound operator, however several image sharpness metrics have been developed which can be used to automate image sharpness as a function of SoS. Treeby, Varslot, Zhang, Laufer, and Beard (2011) detail the performance of several image focus metrics (normal variance, lateral energy, spatial energy, Brenner sharpness and Tenenbaum sharpness) applied to imaging a tissue phantom with a known sound speed and *in-vivo* measurements of the vasculature in the flank of an adult mouse. Estimation of the average SoS in tissue using image sharpness metrics can readily be automated, making this a suitable for technique to pursue for real time estimates of fat content in meat of both live animals and carcasses. Limitations of image sharpness techniques are that the contribution of layers of tissue, such us subcutaneous fat, are difficult to remove from the overall estimation of SoS. For animal measurements this could mean that the subcutaneous fat depth needs to be corrected for before accurate IMF% can be estimated. Methods have been developed which address layers of tissue with differing SoS, such as image deconvolution (Shin, Prager, Gomersall, Kingsbury, Treece, & Gee, 2010).

Recent work, primarily driven by the needs of medical ultrasound imaging and diagnoses have resulted in the development of novel SoS mapping techniques. SoS mapping has been developed to improve ultrasound image focus and as a disease diagnostic tool. An example is diagnosis of fatty liver disease, where the speed of sound observed in fatty livers is approximately 40m/s lower than that of healthy liver (Ghoshal, Lavarello, Kemmerer, Miller, & Oelze, 2012; Sehgal, Brown, Bahn, & Greenleaf, 1986). SoS mapping techniques provide a pixel-by-pixel estimate of

the SoS of an image in real time. Jaeger, Held, Peeters, Preisser, Grünig, and Frenz (2015) introduced a novel method termed Computed Ultrasound Tomography in Echo mode (CUTE). CUTE uses a standard ultrasound imaging setup and estimates the SoS of each pixel by calculating the phase aberrations from the expected arrival time given that the speed of sound is not uniform in most samples. This technique was refined in further publications to reduce artefacts in the SoS image reconstruction. Notably, Stähli, Frenz, and Jaeger (2021) used a Bayesian approach to CUTE with a priori segmentation of tissue layers to greatly reduce SoS image clutter.

Evidence from medical ultrasound research indicates that B-mode ultrasound can be used to determine the speed of sound, and therefore fat content, of tissue through a variety of techniques. Further, these techniques can be implemented in existing ultrasound scanning systems as no change of hardware is required, indicating a potentially rapid uptake by the industry.

Publications

Table 1: review of published work on ultrasound measurements of intramuscular fat.

Reference	Method	Summary
A-Mode		
H.-J. Young, N. T. Jenkins, Q. Zhao, and K. K. Mccully (2015)	US Echo intensity	Need to correct for subcutaneous fat. Compared to MRI estimates of IMF%
Bradbury (2007)	Penetrating probe	Good correlations with IMF%, not suitable for live animals.
B-mode		
Napolitano, Chou, McLaughlin, Ji, Mo, DeBusschere, and Steins (2006)	Focus	Clinical images, varied speed of sound parameter to increase spectral energy
Nebeker and Nelson (2012)	Pulse Echo	Reflection mode, required a strong reflector such as
Qu, Azuma, Liang, and Nakajima (2012)	Speckle pattern	Speckle is due to local differences in speed of sound.
Treeby et al. (2011)	Focus	Autofocus of photoacoustic data

Jakovljevic, Hsieh, Ali, Chau Loo Kung, Hyun, and Dahl (2018)	Pulse Echo	Model based approach to speed of sound estimates of traditional ultrasound images.
(Pirmoazen, Khurana, El Kaffas, & Kamaya, 2020)	Attenuation	The attenuation of ultrasound was used to diagnose fatty liver disease
Jaeger, Robinson, Akarçay, and Frenz (2015)	CUTE	First instance of Computed Ultrasound Tomography in Echo mode
Jaeger and Frenz (2015)	CUTE	Artefact reduction in CUTE images
Li, Duric, Littrup, and Huang (2009)	Ultrasound tomography	Breast cancer detection, improved edge detection.

Background and additional references

Chambaz, Dufey, Kreuzer, and Gresham (2002)	Ultrasound in live cattle	Discussion on factors influencing IMF estimate using ultrasound scanning
Samara, Ventura, Alfadda, and Goran (2012)	MRI fat measurements	Reference accuracy measurements
Anderson, McKeag, and Trahey (2000)	Ultrasound speed of sound	Quantification of imaging errors based on speed of sound variation
Ma (2008)	MRI Dixon method	Water and Fat suppression in MRI imaging
Duck (1990)	US properties in tissues	Reference values of sound speed in various tissues
(Deng, Rouze, Palmeri, & Nightingale, 2016)	Shear wave	Overview of Verasonics ultrasound system
Schiefler, Maia, Schneider, Zimbico, Assef, and Costa (2018)	Plane wave imaging	General overview of Plane wave imaging

2 Method

2.1 Samples

Five frozen/thawed New Zealand lamb saddles and three fresh Wagyu beef loins with marble scores ranging from 1-8 were used for ultrasound imaging. Lamb saddles also had MRI images collected for comparison to ultrasound data. Wagyu loins were cut into three sections approximately 20cm in length and vacuum packed. To date one section from each marble grade has been imaged. The remaining 6 have been stored for future scanning. Unfortunately, lockdown policies at the University of Auckland prevented scanning of these loins within the timeframe of this report. Each loin was imaged at approximately 25mm spacing resulting in approximately 7 image locations depending on the loin length. Intramuscular fat percentage was measured at these locations using an NIR prediction model of the homogenised, freeze-dried powder. *Figure 1* shows the intramuscular fat content of each saddle/loin in order of median IMF%. The lamb saddle IMF% were higher than is typical for New Zealand lamb, possibly due to water loss through the thawing/warming process.
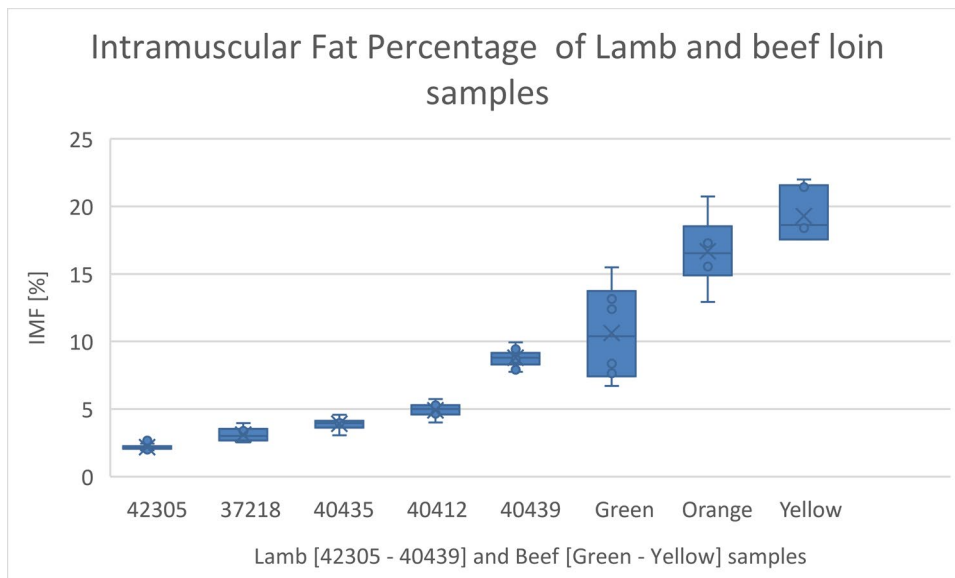

Figure 1: Intramuscular fat [IMF%] content of intact beef loin and lamb saddles in order of mean IMF%.

2.2 Dixon method MRI Imaging

The Dixon method is an MRI imaging protocol designed to uniformly supress fat or water. The Dixon technique exploits the fact that water and fat molecules precess at different rates in a strong magnetic field. Over time, fat and water will alternate between being in and out of phase. Acquiring both in-phase and out-of-phase images simultaneously allows the images to be combined mathematically resulting in a total of 4 images per scan:

In-phase = (water + fat)

Out-of-phase = (water - fat)

Fat only = In-phase - Out-of-phase = (water + fat) - (water - fat)

9

Water only = In-phase + Out-of-phase = (water + fat) + (water - fat)

Images were collected at the Centre for Advanced Magnetic resonance imaging (CAMRI). Loins were warmed to room temperature and imaged using the 'head' coil. Images slices are collected as horizontal cross sections at a resolution of 0.69 x 0.69 mm. The spacing between vertical slices was set to 0.7mm, resulting in nearly square voxels for each 3D volume.

3 Ultrasound

Body temperature (37ºC) lamb and beef saddles with a range of marble scores were used as a proxy for live animal measurements. A plane wave imaging protocol was used to collect raw ultrasound data at 2.5cm intervals on the surface of the saddle, resulting in approximately 7 scanning locations per loin. Images were collected transversally such that a each image resulted in a cross-section perpendicular to the muscle fibre orientation. Data was collected using a Verasonics Vantage 128 with two probes, discussed in section 0. A plane wave imaging protocol was used to collect raw ultrasound data. 40 angles were used from -30 to +30 degrees to the normal of the surface. Figure 2 shows a schematic of conventional and plane wave imaging.
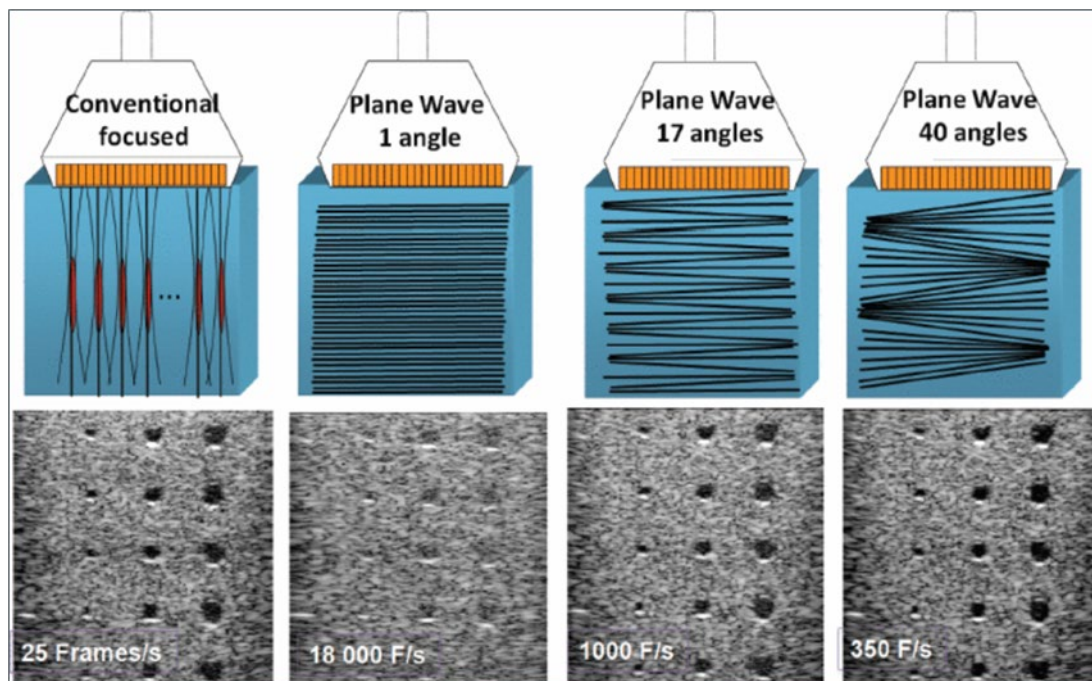

Figure 2: Example of Conventional focused ultrasound imaging and Plane Wave imaging at various number of angles. Plane wave imaging is much faster than focussed imaging and allows for novel reconstruction methods to predict speed of sound in real time.
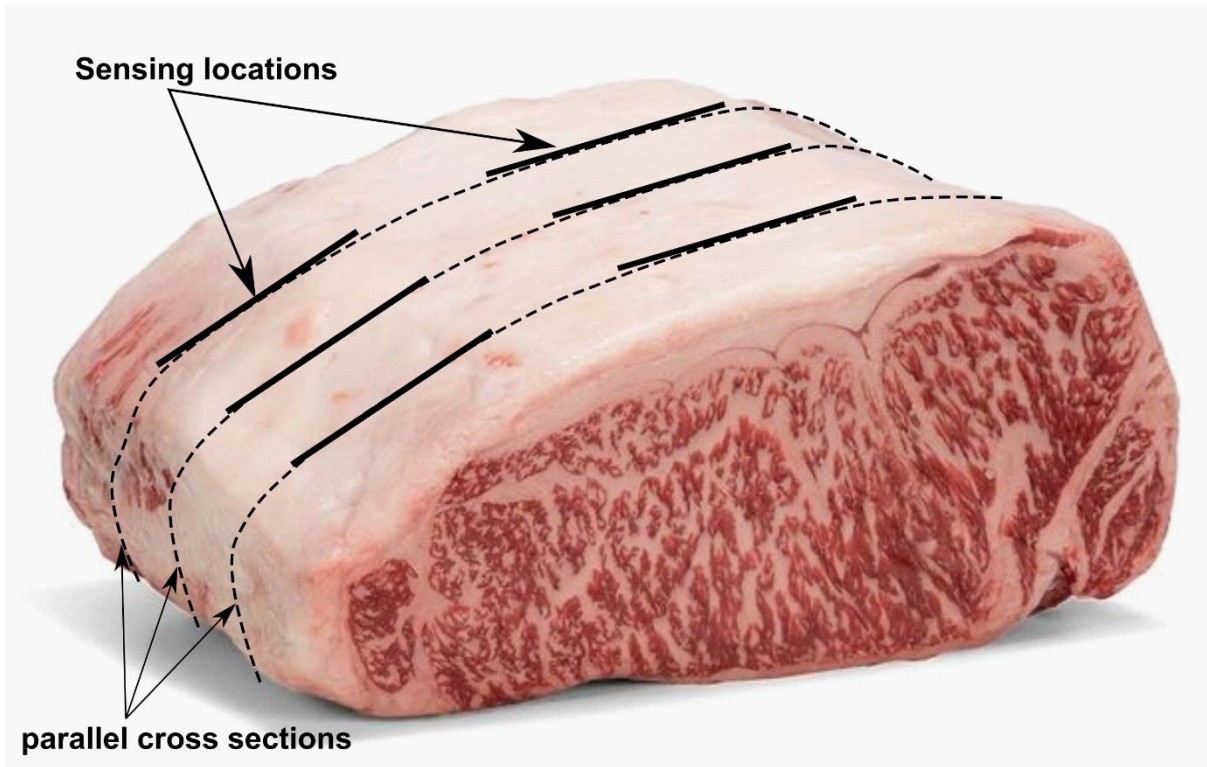
Figure 3: Imaging locations on the wagyu beef loin. For the samples used in this study the bones and fat cap were not removed.

3.1 Probes

Many ultrasound probes have been developed for various imaging applications depending on the required image resolution, field of view, penetration depth etc. Higher frequency ultrasound experiences more scattering and therefore can be used to reproduce images at a higher resolution. However greater scattering reduces the penetration depth of ultrasound waves and therefore reduced image depth. Further, higher frequency probes require smaller element sizes which reduce the sensitivity. Two probes were used to collect ultrasound data in this study 1) the 6MHz L11 linear array and 2) 3MHz P4 phased array. Specifications of each probe are given below:

The L11 128-element linear array transducer
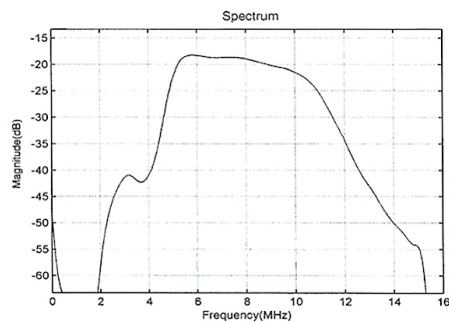
Number of elements	128
Pitch (mm)	0.3
Elevation focus (mm)	18
Sensitivity (dB)	-52 ±3
Compatibility	All Standard and High Frequency Configurations of the Vantage Systems

The P4-2v 64-element phased array transducer
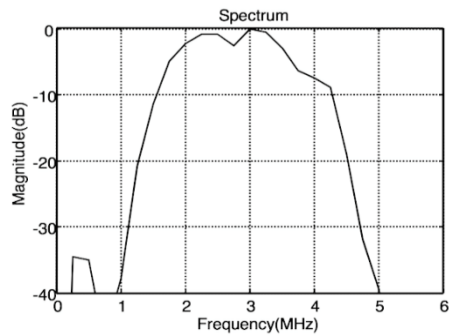
Number of elements	64
Pitch (mm)	0.3
Elevation focus (mm)	50-70
Sensitivity (dB)	-69 -95
Compatibility	All Standard and High Frequency Configurations of the Vantage

1.1 Temperature control

Speed of sound in both fat and muscle is highly dependent on temperature. Previous work showed that in beef loin at a temperature of 37ºC fat had a SoS of ~ 1440m/s and muscle had a SoS of ~1580m/s. It was also shown that the SoS of muscle and fat were equal at approximately 15ºC, meaning that SoS cannot be used to estimate IMF content. At lower temperatures fat has a higher speed of sound than muscle, reversing previous correlations between SoS and fat content. Samples used in this study were warmed in a 37ºC water bath for approximately 2 hours before imaging. Samples were imaged in the waterbath to ensure that temperature did not change over the course of the data collection. Unfortunately warming of the vacuum bags often caused the bags to open and allow water in. It is not known how this has impacted the speed of sound images.

4 Results

4.1 MRI

4.1.1 Averaging, Filtering and Normalising

Averaging is used to improve SNR of collected images at the cost of imaging time. Saddle 40436 was used to assess image quality using two, four and six averages (*Figure 4*). It was found that in all images 'banding' was occurring due to each horizontal slice being filtered using an elliptical filter and normalised. In a latter session, saddle 40439 was used to minimise the effect of this banding using different combinations of normalisation and filtering. It was found that two averages and no normalisation or elliptical filtering produced most consistent images for reconstruction of 3D models of lamb saddles.
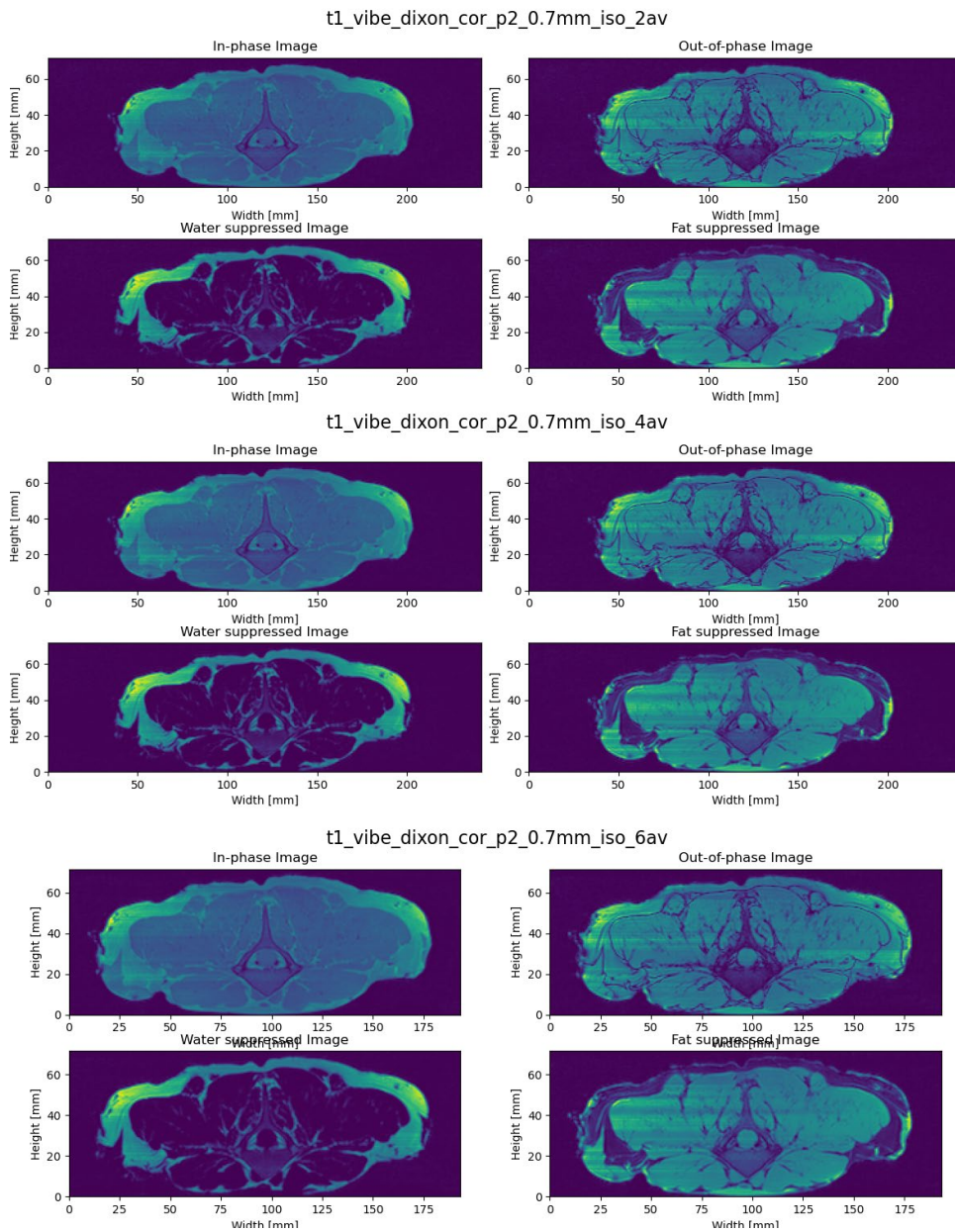
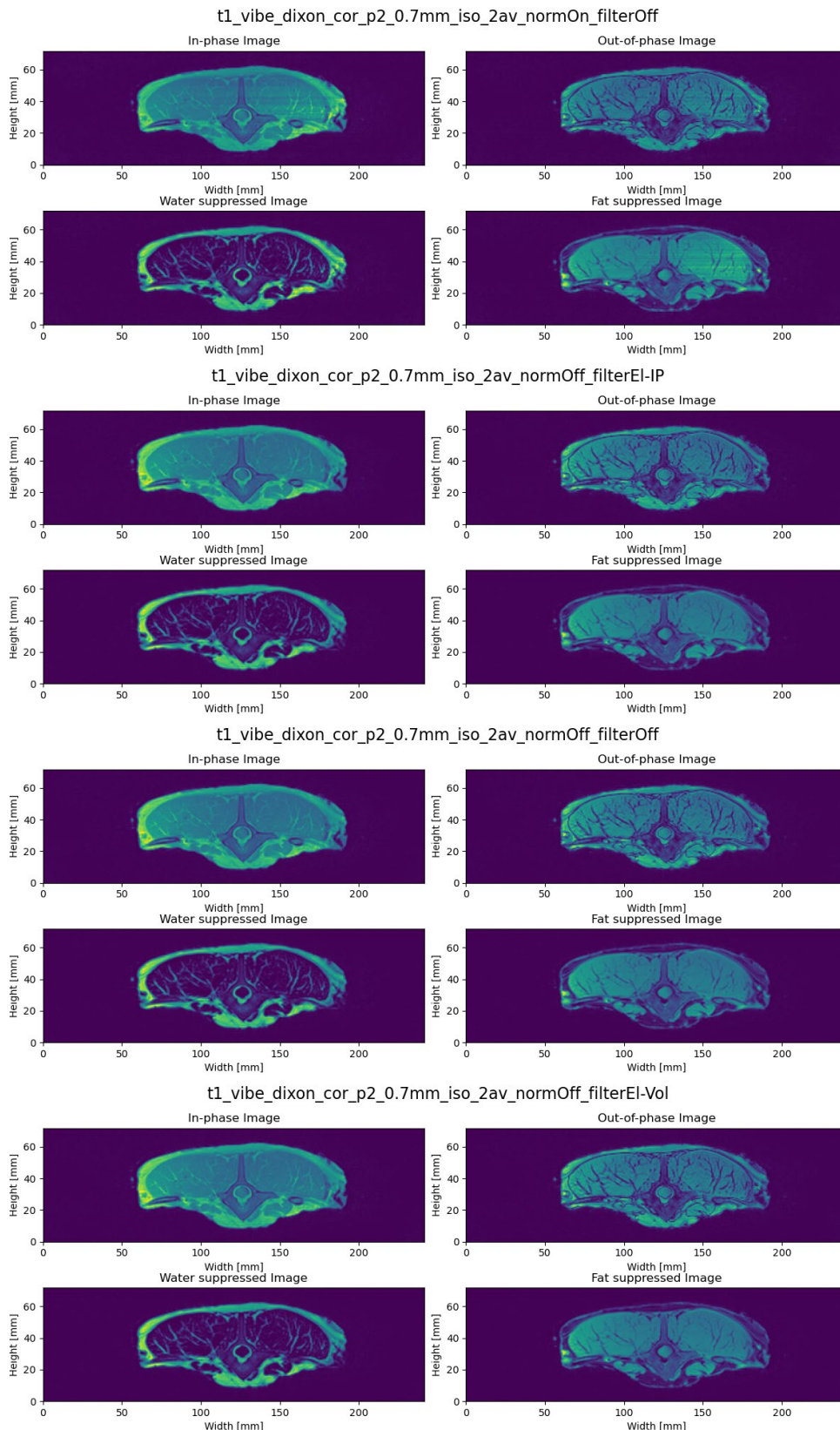*Figure 4: Cross sections of saddle 40436 collected using the Dixon method with 2,4 and 6 averages.*

Figure 5: Cross sections of saddle 40439 collected using the Dixon method with varying combinations of filtering and normalisation.

MRI imaging of subsequent loins

The remaining saddles were imaged using the optimised Dixon imaging protocol. Figures 6-9 show cross sections of saddles at a range of marble scores.
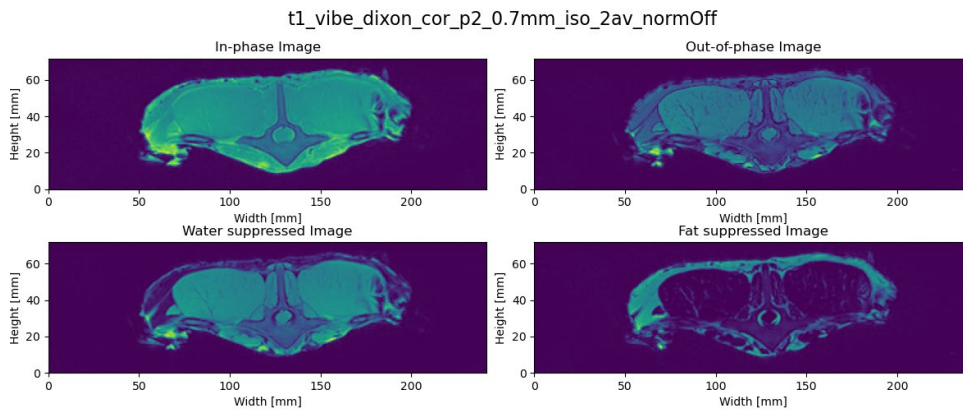

Figure 6: Cross sections of saddle 40435 collected using the optimised Dixon method
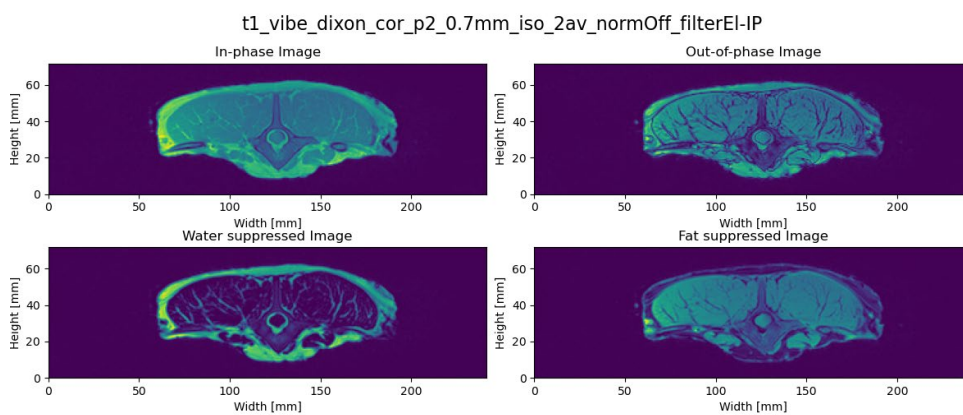

Figure 7: Cross sections of saddle 40439 collected using the optimised Dixon method
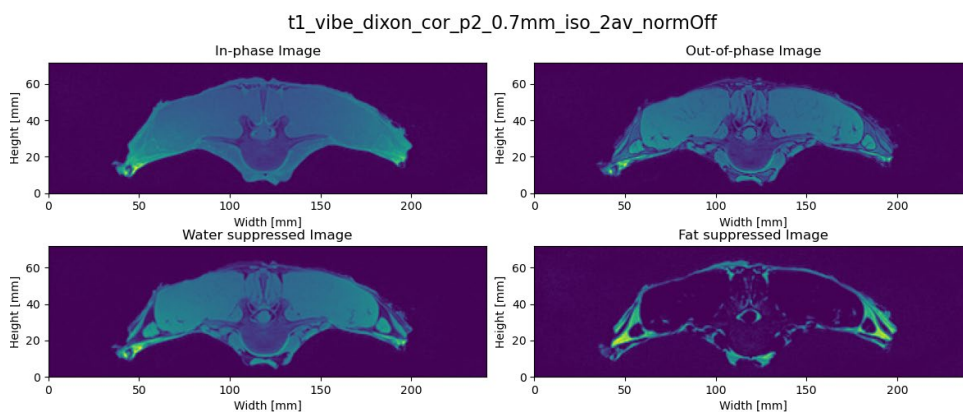
37218

Figure 8: Cross sections of saddle 37218 collected using the optimised Dixon method
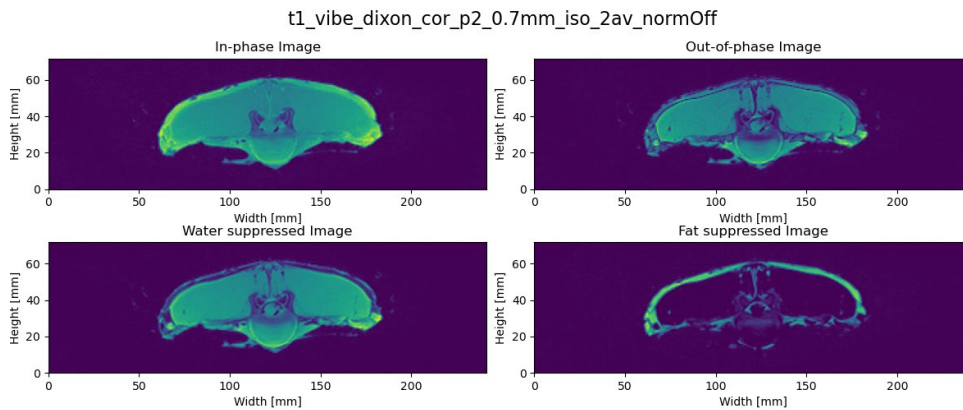

Figure 9: Cross sections of saddle 42305 collected using the optimised Dixon method

4.2   MRI Image segmentation

The image contrast between fat, water and bone of MRI data collected using the Dixon method allows for pixels to be classified using simple thresholding and morphological smoothing techniques. Once segmented, each image can be assigned appropriate physical parameters, for example density and speed of sound, based on the pixel classification. Applying this to each cross-section collected along the length of a saddle results in a full recreation of the saddle with assigned physical parameters which can be used to simulate ultrasound imaging techniques. K-wave (http://www.k-wave.org/) is an open-source acoustics toolbox developed for MATLAB. The software is designed for time domain acoustic and ultrasound simulations in complex and tissue-realistic media. Figure 10 shows an example of a fat suppressed image which has been segmented into various tissue types.
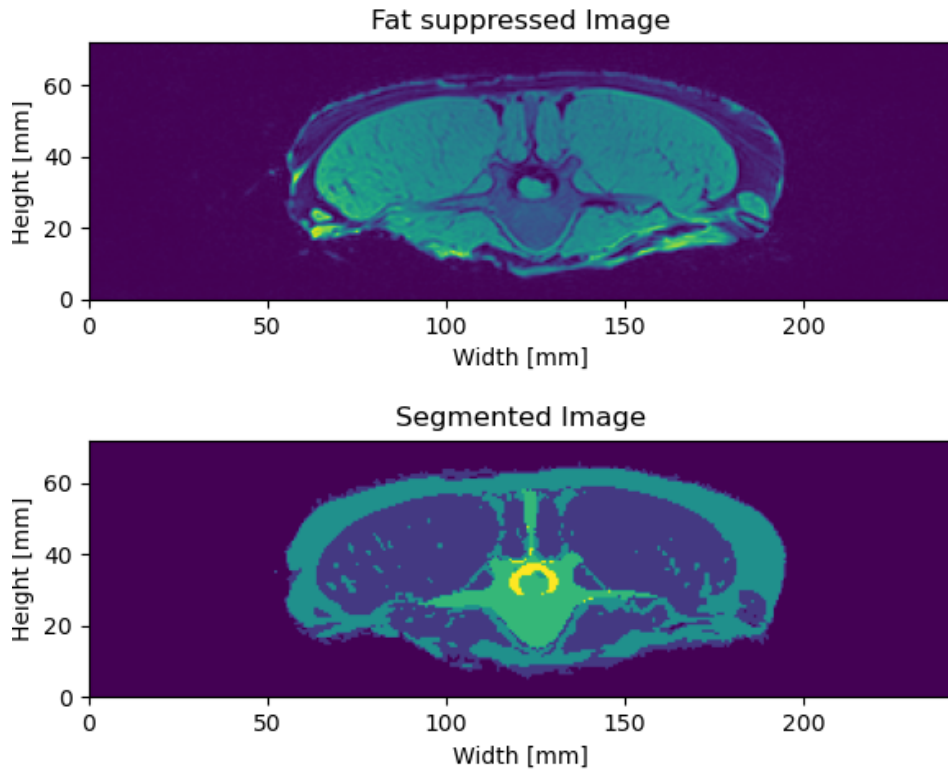
Figure 10 Fat suppressed Image and the corresponding image segmented into fat, muscle, bone, and marrow.
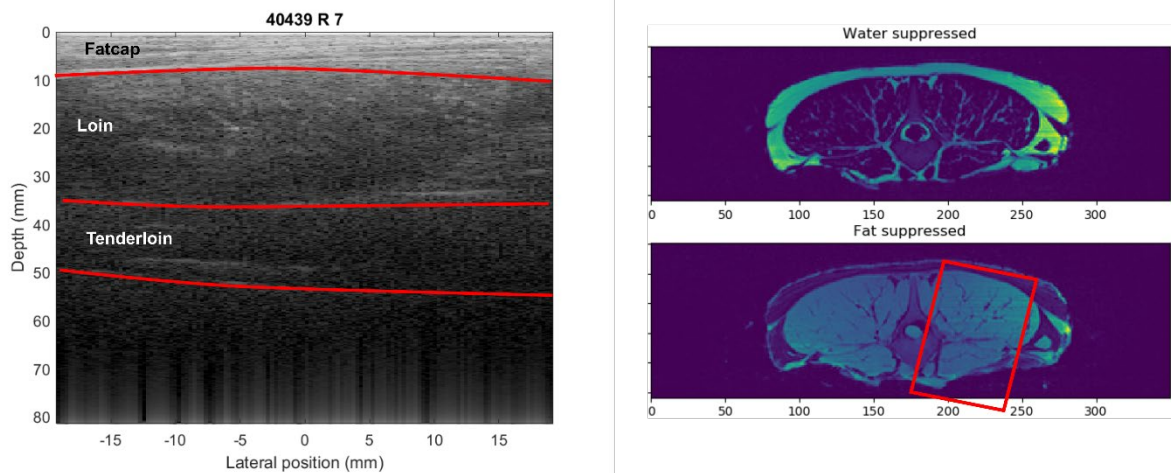
4.3 Ultrasound

Figure 11 Comparison between MRI and Plane wave ultrasound images collected at approximately the same location on a lamb loin. Right) The red box indicates approximately where the ultrasound image was collected.

5 Speed of sound metrics

Following Treeby et al. (2011), image sharpness metrics were used to estimate the average SoS of each image collected on each lamb loin. In the following sections the estimated speed of sound is plotted as a function of marble score (section 5.1) and IMF (section 5.2 and 5.3).

5.1 Correlation between Average SoS and marble score

To visualise the correlation with visual marble score, the SoS estimates collected for each lamb were averaged and plotted against the visual marble score (Figure 12). Of the metrics assessed lateral energy, Brenner and Tenenbaum sharpness had the strongest correlation with marble score. As discussed by Treeby et al. (2011), the Brenner sharpness metric is most sensitive to tissue SoS, so it is not surprising that SoS estimated by this metric is highly correlated with increasing fat.
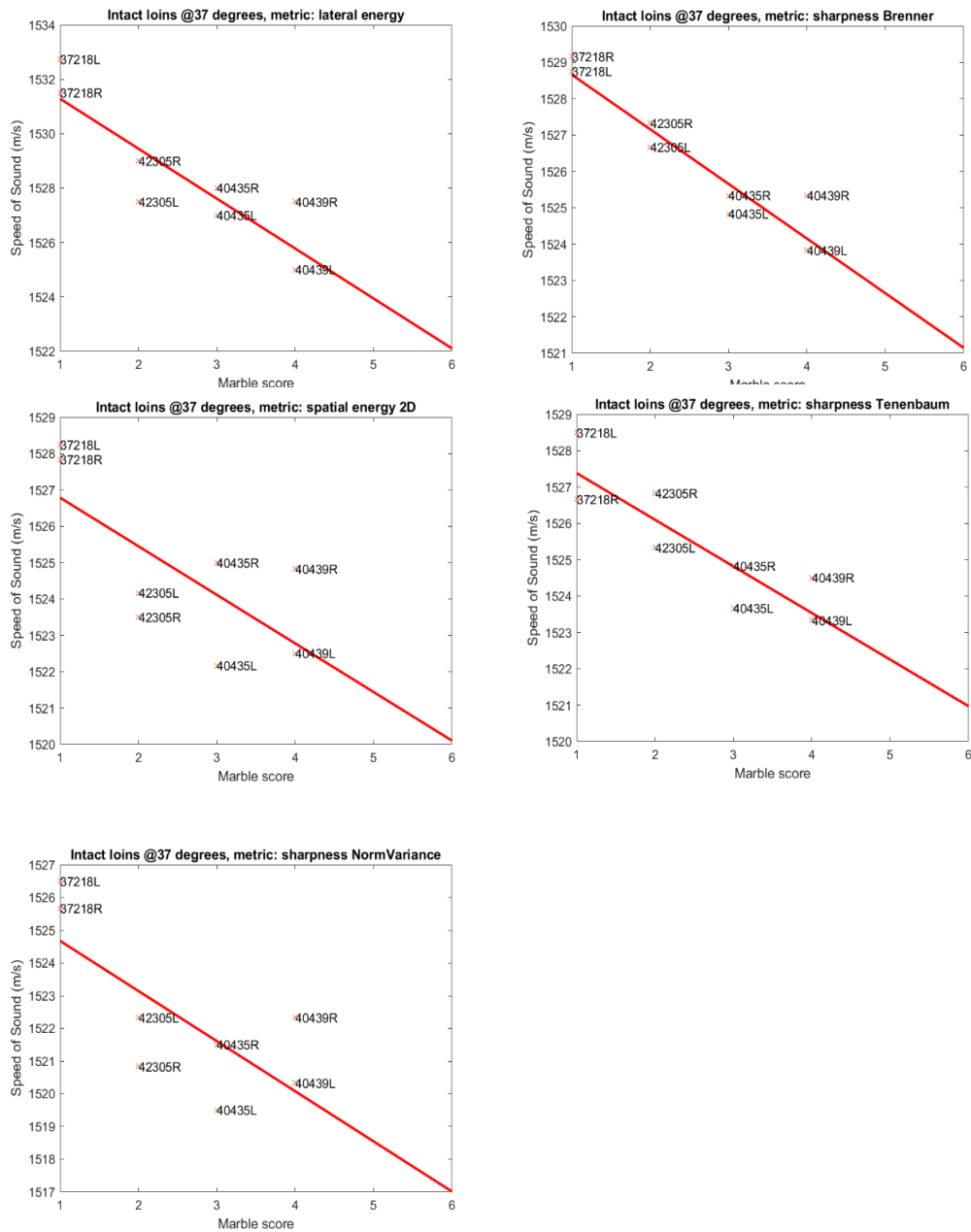
Figure 12: Average speed of sound predicted using several sharpness metrics plotted against the visual marble score for each loin.

5.2   Correlation between SoS and IMF% per image:

Using the image sharpness metrics the SoS of each image was calculated and plotted against IMF% (Figure 13). The steepest relationship between estimated SoS and IMF% was found using the lateral energy sharpness metric, followed by Brenner and Tenenbaum metrics. However, there is a significant range in estimated SoS for similar estimates of IMF%. It is unclear if the range of SoS predicted values is due to poor image quality or inconsistent imaging conditions.
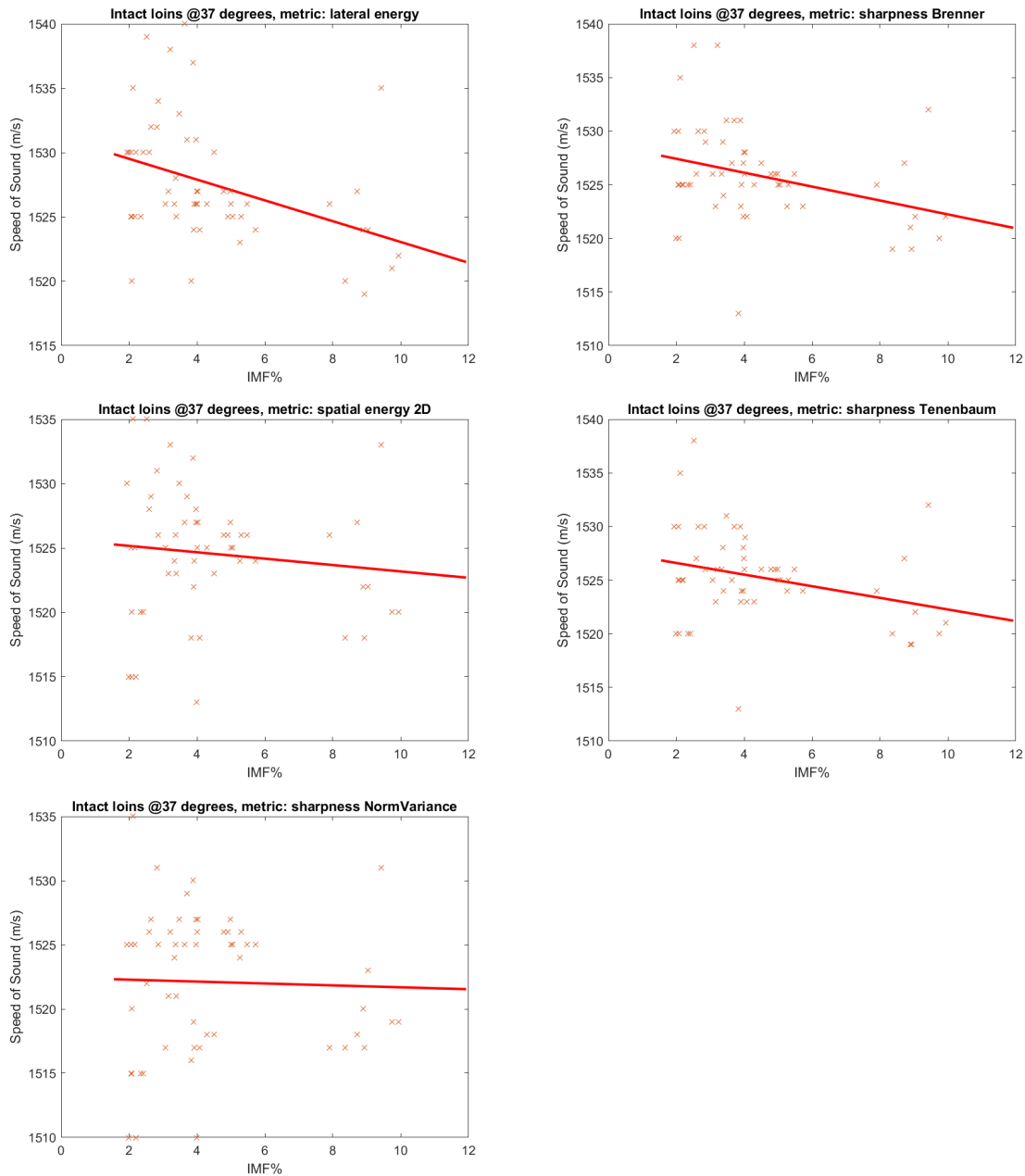

Figure 13: Loin SoS estimated using sharpness metrics for each loin location plotted against IMF% for each image.

5.3   Example of SoS estimates in a single loin

Figure 14 shows the SoS estimates using sharpness metrics at several locations on a single loin. Lateral energy showed no correlation with IMF%, however other metrics estimated lower speed of sound with increasing IMF% which agrees with previous literature. The SoS estimate from the second lowest IMF% location is consistently lower than its nearest neighbours. This suggests a poor image capture at this location.
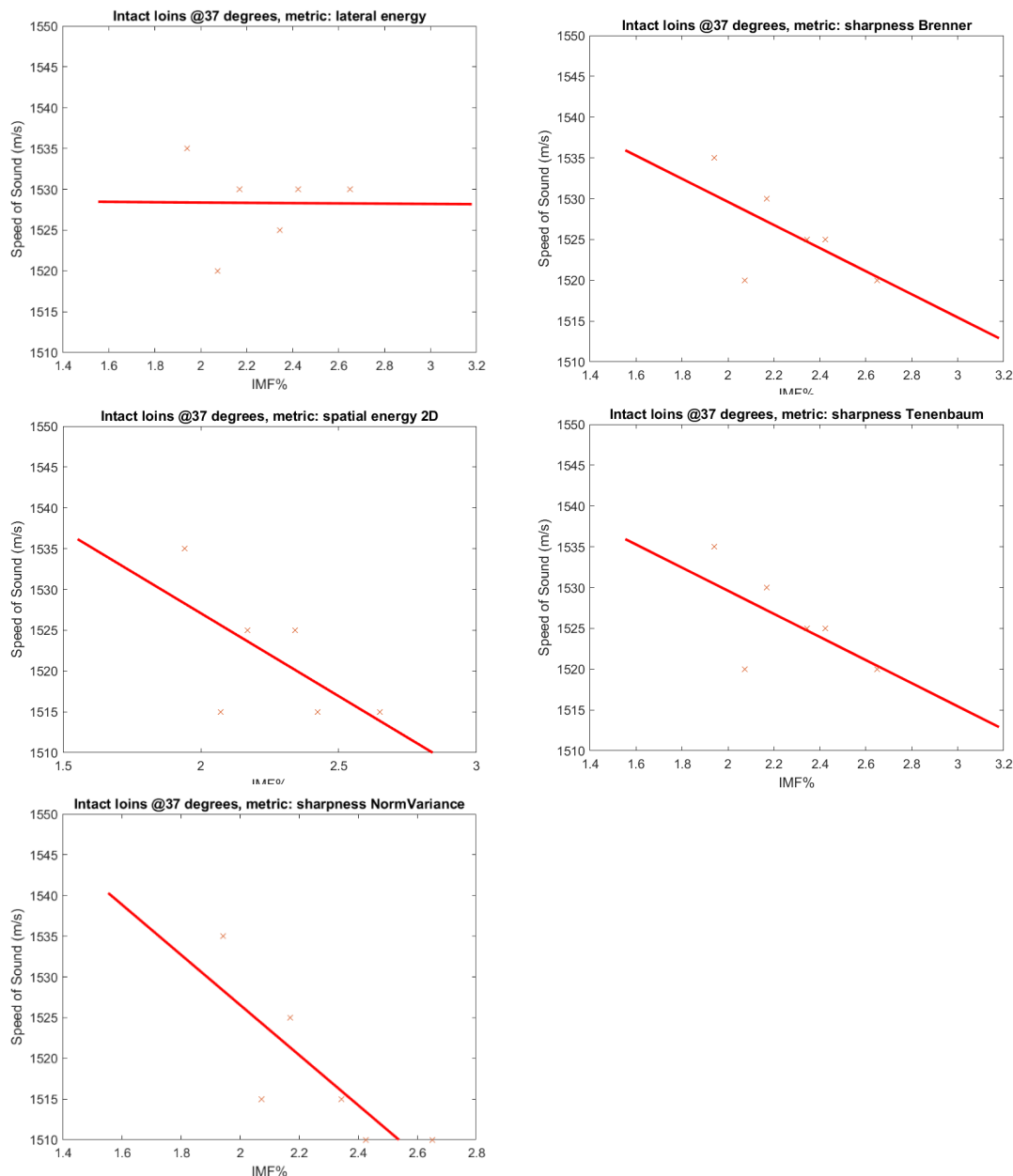

Figure 14: SoS estimates of loin 42305L using sharpness metrics.

6   Discussion

It is clear from previous literature and industry reports that there are many avenues to explore IMF% estimation using measurements of speed of sound in meat. Primarily driven by the needs

of the medical industry, many research articles have been recently published which address speed of sound measurements using both A- and B-mode ultrasound. Due to the acoustic properties of fat and muscle, SoS estimates with standard ultrasound hardware could provide an automated, objective means of IMF% estimation in live animals and pre-chiller carcasses.

During this work raw ultrasound data and MRI images were collected on the same intact loin samples with a wide variation in IMF% for the first time. This dataset provides a foundation which can be used to explore the many potential techniques of muscle assessment. Most of the methods for estimating SoS, and therefore IMF%, must be conducted before an image is reconstructed, which means that raw ultrasound data is required. The Physical Acoustics Laboratory at the University of Auckland has equipment and expertise to assist in gathering preliminary data outlined in this report, however the laboratory is not suitable for large scale animal or carcass trials. To allow for these trials to commence, which are required before commercialising can occur, a portable device which can be deployed in plant or farm is required.

For the analyses explored in this work a focus was placed on methods of SoS estimation which could be automated with relative ease and provide an objective estimate the average the SoS of the loin muscle. Of these techniques optimising image sharpness by varying the value of SoS during image reconstruction has been previously explored in the literature with good results. Initial work showed that the SoS, which was calculated by obtaining SoS estimates along the length of the loin with a variety of sharpness metrics, was inversely correlated with visual marble score. Of the image sharpness metrics used to estimate the SoS, lateral energy, Brenner and Tenenbaum sharpness metrics showed particularly good correlations with marble score. The difference in SoS between the marble score 1 (32718) and marble score 4 (40439) is approximately 5 ms^{-1} for the Tenenbaum and Brenner metrics, which is in agreement with the theoretically estimated value based on the difference in IMF% of these loins.

When examining the relationship between estimated SoS and IMF% of each collected image the correlation is much weaker than in the case of average SoS and marble score. Though most image sharpness metrics showed a decreasing SoS with increasing IMF% when considering the line of best fit, there is a wide range of estimated SoS for similar estimates of IMF%. Variation in measurements could be due to environmental factors such as muscle temperature control, or poor coupling between the transducer and muscle resulting in low quality images. Using loin 42305L as an example, the relationship between IMF% and SoS was examined using data collected under the same conditions. With the exception of a single SoS estimate that appears to be underestimating the SoS of the loin, these figures showed a much stronger correlation than the bulk figure. This suggests that the poor correlation between SoS and IMF% across all loins is due to loin-to-loin conditions. Further work would be required to determine if this is due to intrinsic conditions of the loin, or experimental conditions of these trials/analyses. Interestingly the lateral energy metric showed the greatest sensitivity to IMF% when considering SoS estimates for all data (Figure 13), but almost no correlation when considering SoS estimates within a single loin (Figure 14). This suggests that certain metrics could be used to account for environmental conditions while others are used to predict IMF%.

These findings indicate that new algorithms and imaging protocols could be implemented on existing hardware, providing the industry with improved decision support tools for grading live animals. In order to validate these findings in a commercial setting a device should be

23

developed which can be deployed on-farm or in-plant. Our team at Agresearch ltd has extensive experience in translating off the shelf components to a deployable system. Alongside development of the system, end users of the device should be consulted, and the needs of the red meat industry refined on the road to a final design.

7 Citation

Anderson, M., McKeag, M., & Trahey, G. (2000). The impact of sound speed errors on medical ultrasound imaging. *The Journal of the Acoustical Society of America, 107*(6), 3540-3548.

Bradbury, R. (2007). Development proposal for Velocity of Sound (VOS) marbling probe

(Proof of concept). *A.MQT.0026*.

Chambaz, A., Dufey, P.-A., Kreuzer, M., & Gresham, J. (2002). Sources of variation influencing the use of real-time ultrasound to predict intramuscular fat in live beef cattle. *Canadian journal of animal science, 82*(2), 133-139.

Deng, Y., Rouze, N. C., Palmeri, M. L., & Nightingale, K. R. (2016). Ultrasonic shear wave elasticity imaging sequencing and data processing using a verasonics research scanner. *IEEE transactions on ultrasonics, ferroelectrics, and frequency control, 64*(1), 164-176.

Duck, F. A. (1990). Chapter 4 - Acoustic Properties of Tissue at Ultrasonic Frequencies. In F. A. Duck (Ed.), *Physical Properties of Tissues* (pp. 73-135). London: Academic Press.

Jaeger, M., & Frenz, M. (2015). Towards clinical computed ultrasound tomography in echo-mode: Dynamic range artefact reduction. *Ultrasonics, 62*, 299-304. doi: https://doi.org/10.1016/j.ultras.2015.06.003

Jaeger, M., Held, G., Peeters, S., Preisser, S., Grünig, M., & Frenz, M. (2015). Computed Ultrasound Tomography in Echo Mode for Imaging Speed of Sound Using Pulse-Echo Sonography: Proof of Principle. *Ultrasound in Medicine & Biology, 41*(1), 235-250. doi: https://doi.org/10.1016/j.ultrasmedbio.2014.05.019

Jaeger, M., Robinson, E., Akarçay, H., & Frenz, M. (2015). Full correction for spatially distributed speed-of-sound in echo ultrasound based on measuring aberration delays via transmit beam steering. *Physics in medicine and biology, 60*, 4497-4515. doi: 10.1088/0031-9155/60/11/4497

Jakovljevic, M., Hsieh, S., Ali, R., Chau Loo Kung, G., Hyun, D., & Dahl, J. J. (2018). Local speed of sound estimation in tissue using pulse-echo ultrasound: Model-based approach. *The Journal of the Acoustical Society of America, 144*(1), 254-254. doi: 10.1121/1.5043402

Kim, S., & Khambampati, A. K. (2015). 12 - Mathematical concepts for image reconstruction in tomography. In M. Wang (Ed.), *Industrial Tomography* (pp. 305-346): Woodhead Publishing.

Li, C., Duric, N., Littrup, P., & Huang, L. (2009). In vivo breast sound-speed imaging with ultrasound tomography. *Ultrasound in medicine & biology, 35*(10), 1615-1628. doi: 10.1016/j.ultrasmedbio.2009.05.011

Ma, J. (2008). Dixon techniques for water and fat imaging. *Journal of Magnetic Resonance Imaging, 28*(3), 543-558. doi: https://doi.org/10.1002/jmri.21492

Napolitano, D., Chou, C.-H., McLaughlin, G., Ji, T.-L., Mo, L., DeBusschere, D., & Steins, R. (2006). Sound speed correction in ultrasound imaging. *Ultrasonics, 44*, e43-e46. doi: https://doi.org/10.1016/j.ultras.2006.06.061

Nebeker, J., & Nelson, T. R. (2012). Imaging of Sound Speed Using Reflection Ultrasound Tomography. *Journal of Ultrasound in Medicine, 31*(9), 1389-1404. doi: 10.7863/jum.2012.31.9.1389

Park, B., Whittaker, A. D., Miller, R. K., & Hale, D. S. (1994). Predicting intramuscular fat in beef longissimus muscle from speed of sound. *Journal of Animal Science, 72*(1), 109-116. doi: 10.2527/1994.721109x

Pirmoazen, A. M., Khurana, A., El Kaffas, A., & Kamaya, A. (2020). Quantitative ultrasound approaches for diagnosis and monitoring hepatic steatosis in nonalcoholic fatty liver disease. *Theranostics, 10*(9), 4277-4289. doi: 10.7150/thno.40249

Qu, X., Azuma, T., Liang, J. T., & Nakajima, Y. (2012). Average sound speed estimation using speckle analysis of medical ultrasound data. *International Journal of Computer Assisted Radiology and Surgery, 7*(6), 891-899. doi: 10.1007/s11548-012-0690-9

Samara, A., Ventura, E. E., Alfadda, A. A., & Goran, M. I. (2012). Use of MRI and CT for fat imaging in children and youth: what have we learned about obesity, fat distribution and metabolic disease risk? *Obesity Reviews, 13*(8), 723-732. doi: 10.1111/j.1467-789X.2012.00994.x

Schiefler, N. T., Jr., Maia, J. M., Schneider, F. K., Zimbico, A. J., Assef, A. A., & Costa, E. T. (2018). Generation and Analysis of Ultrasound Images Using Plane Wave and Sparse Arrays Techniques. *Sensors (Basel, Switzerland), 18*(11), 3660. doi: 10.3390/s18113660

Shin, H.-C., Prager, R., Gomersall, H., Kingsbury, N., Treece, G., & Gee, A. (2010). Estimation of speed of sound in dual-layered media using medical ultrasound image deconvolution. *Ultrasonics, 50*(7), 716-725. doi: https://doi.org/10.1016/j.ultras.2010.02.008

Stähli, P., Frenz, M., & Jaeger, M. (2021). Bayesian Approach for a Robust Speed-of-Sound Reconstruction Using Pulse-Echo Ultrasound. *IEEE Transactions on Medical Imaging, 40*(2), 457-467. doi: 10.1109/TMI.2020.3029286

Treeby, B., Varslot, T., Zhang, E., Laufer, J., & Beard, P. (2011). Automatic sound speed selection in photoacoustic image reconstruction using an autofocus approach. *Journal of Biomedical Optics, 16*(9), 090501.

Whittaker, A. D., Park, B., Thane, B. R., Miller, R. K., & Savell, J. W. (1992). Principles of ultrasound and measurement of intramuscular fat. *Journal of Animal Science, 70*(3), 942-952. doi: 10.2527/1992.703942x

Young, H.-J., Jenkins, N. T., Zhao, Q., & Mccully, K. K. (2015). Measurement of intramuscular fat by muscle echo intensity. *Muscle & Nerve, 52*(6), 963-971. doi: 10.1002/mus.24656

Young, H. J., Jenkins, N. T., Zhao, Q., & McCully, K. K. (2015). Measurement of intramuscular fat by muscle echo intensity. *Muscle & nerve, 52*(6), 963-971.

8 Appendix

A-mode ultrasound

A-mode ultrasound generally refers to systems with a single source and receiver pair. In echo mode the same transducer is used as the source and receiver. Images cannot be reconstructed from A-mode data, however the larger transducer size typically results in better signal to noise ratio.
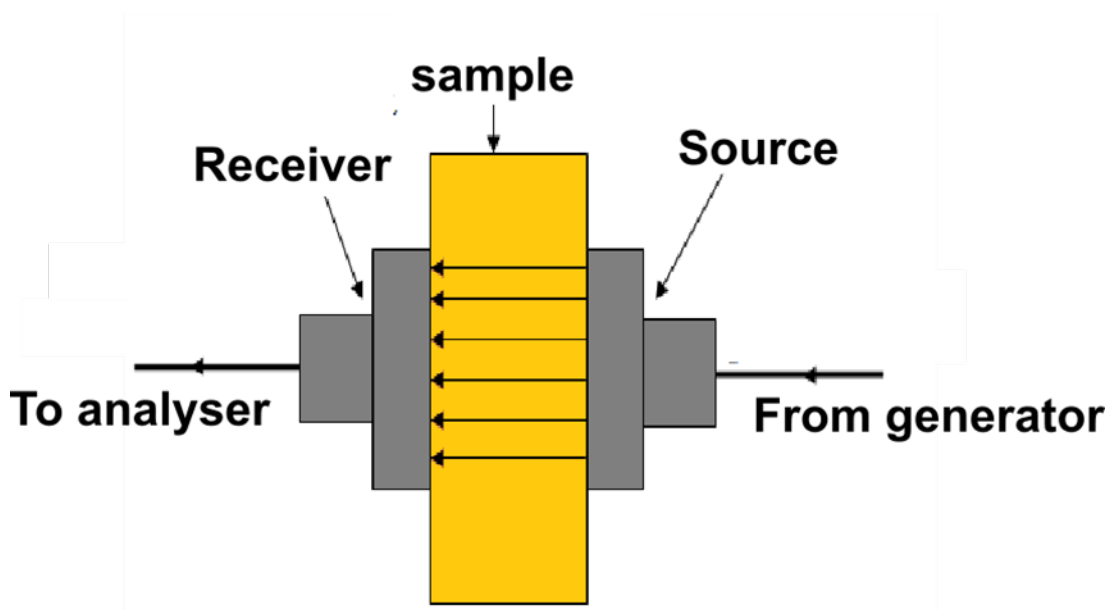

Figure 15: A-mode ultrasound in transmission

Anterior-posterior cross section images

The current ultrasound imaging protocol implemented in New Zealand uses a 5 MHz linear array approximately 10cm long orientated along the length of the loin. Typically, three images are collected and visually assessed for marble score based on image speckle. Imaging an anterior-posterior cross section has the advantage of imaging a larger area of muscle than transverse imaging, however this orientation can not be used by other techniques at the processing line (Hyperspectral imaging, visual marble score assessment). It is unclear whether this is a leading cause of poor correlations between US assessed marble score and other techniques. An example of an anterior-posterior ultrasound image is shown in *Figure 16*. It is the view of the author of this report that anterior-posterior imaging is more likely to miss fat deposits than transverse imaging as intramuscular fat tends to form deposits which run parallel to the muscle fibres. This assumption could be validated using the MRI data which, due to collecting approximately square voxels, can be used to generate cross sections in any orientation. Figures 17-21 show examples of MRI cross sections orientated anterior-posterior using the optimised Dixon imaging protocol.

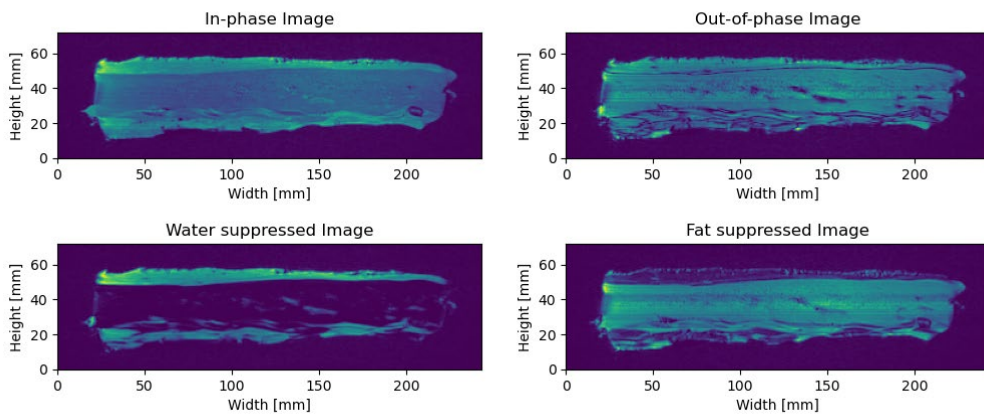*Figure 16: Example of an anterior-posterior cross section ultrasound image collected on a live lamb.*

Figure 17: Anterior-Posterior cross section of saddle 40436
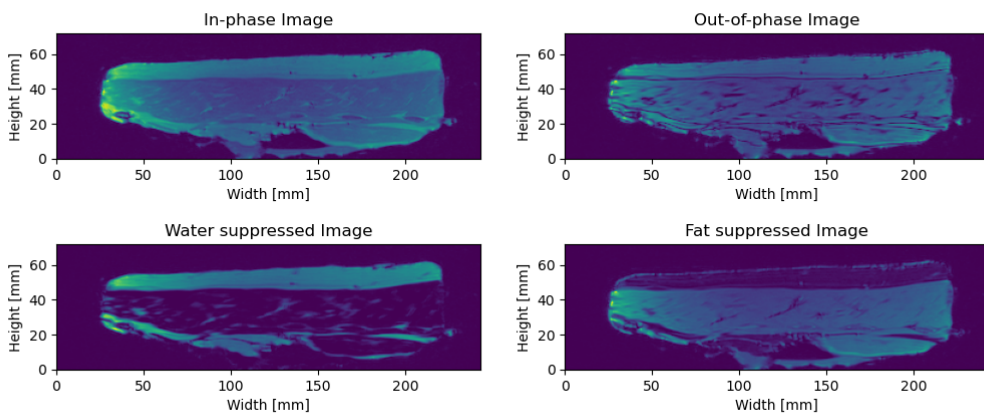
Figure 18: Anterior-Posterior cross section of saddle 40439
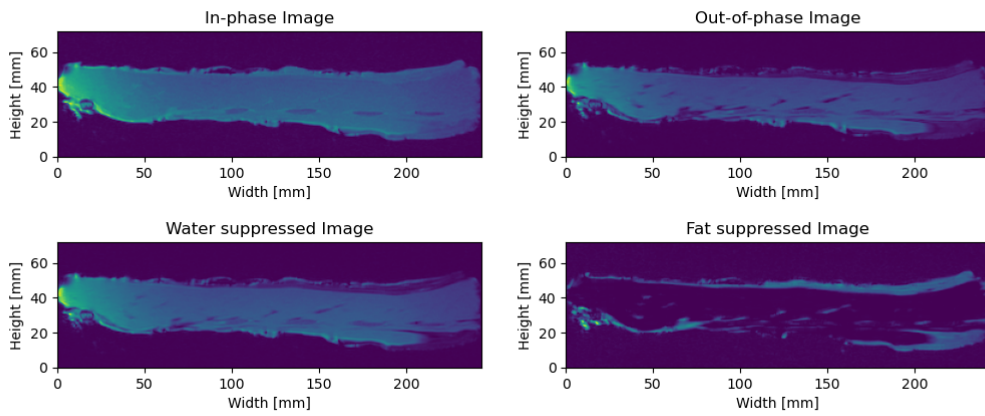
Figure 19: Anterior-Posterior cross section of saddle 37218
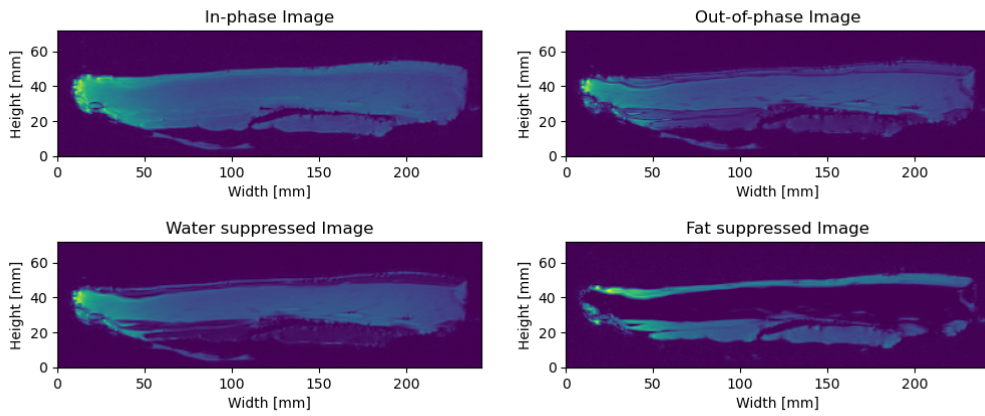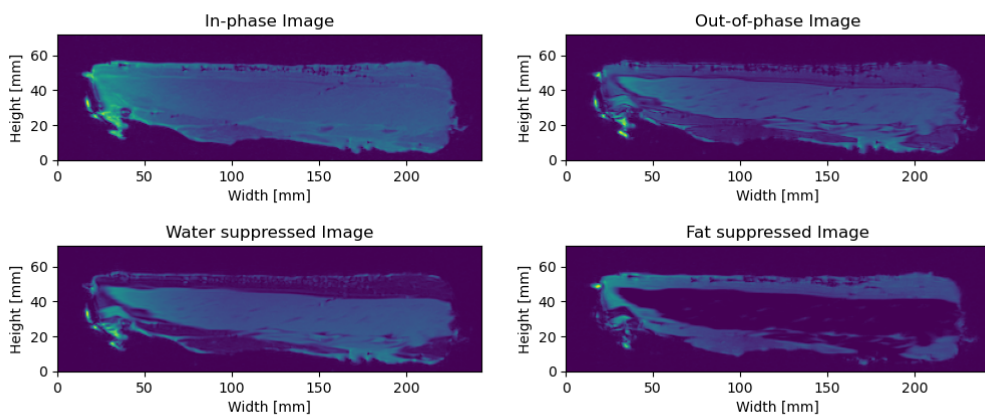

Figure 20:Anterior-Posterior cross section of saddle 42305

Figure 21: Anterior-Posterior cross section of saddle 40435